Final Report on

MCNP Modeling for the UMLRR and Selected Gamma Irradiation Facilities

Dr. John R. White, Russell Gocht, and Michael Ducey

Chemical and Nuclear Engineering Department
University of Massachusetts Lowell
Lowell, MA 01854

September 6, 2011

Introduction/Summary

The primary goal of this project was to develop and validate a detailed MCNP model of the UMass-Lowell Research Reactor (UMLRR) to support the analysis of subsequent experiments within the facility. A secondary task was to also develop and validate MCNP computational models for some of the Co-60 irradiation facilities associated with the UMass-Lowell Radiation Laboratory. This is the Final Report for this project, and it demonstrates full success with both modeling activities. The current documentation implicitly references the previous reports in this series of progress updates and, together, the previous progress reports and this final report fully document the development and validation of all the computational models created as part of this work. In particular, the previous progress updates (Refs. 1-4) focused primarily on describing the MCNP geometric configurations for our reactor modeling efforts and for a model of a Co-60 rack-in-pool experimental arrangement. Selected results were also given in these references, but these were indeed preliminary in nature -- thus, all the final modeling results from the reactor models and from two separate Co-60 irradiation facilities are summarized below in the current document. In contrast, since the reactor geometries and the rack-in-pool geometry have already been summarized in previous reports, that discussion will not be repeated here -- only a brief facility overview will be given.

Thus, the remainder of this report is broken into three primary sections that discuss sequentially the following topics:

1. Validation results for the UMLRR M-1-3 and M-2-5 BOL reactor models and for the M-2-5 model after 50 MWD of burnup,
2. Updated computational results for the Co-60 rack-in-pool geometry, and
3. Calculated flux and dose rate distributions, along with some measured results, for the Co-60 rack and gamma cave irradiation facility. Here we also discuss the MCNP geometry model for the gamma cave since this model was only completed recently and the details were not available within the previous progress reports.

Overall, this project has developed and validated a series of detailed MCNP models for the UMass-Lowell research reactor (UMLRR) and Co-60 irradiation facilities. This new capability significantly enhances our ability to support on-going operations within these facilities and to predict the behavior of new experimental configurations within these irradiation environments.

Validation Results for Various Reactor Configurations

The UMass-Lowell Research Reactor (UMLRR) contains a 7x9 grid of fuel assemblies, graphite reflector elements, radiation baskets, and corner posts. It also has two grid locations reserved for an external neutron source and a low-worth regulating rod for fine reactivity control. Four large control blade assemblies are used for gross reactivity control and for reactor shutdown. From the top view, the reactor is enclosed by an aluminum core box and a large pool of demineralized water surrounds the system on three sides, with a 3 inch lead shield and large graphite thermal column on the remaining side. A specific arrangement of fuel elements, graphite reflector blocks, and radiation baskets make up a particular core configuration.

In August 2000 the UMLRR converted from the use of HEU uranium-aluminide fuel to LEU uranium-silicide fuel (see Refs. 5-8). The basic layout for the LEU startup core arrangement, including the six beam ports and thermal column, is sketched in Fig. 1. This reference configuration is referred to as the M-1-3 core and it contains 19 full fuel assemblies and 2 partial assemblies arranged roughly in the center of the 7x9 grid. Directly in the middle of the core is a central irradiation zone known as the flux trap. The flux trap is similar to a radiation basket, except that the region between the inner irradiation tube and the outer aluminum can is filled with graphite. Note that, when referring to a given location, the row and column indices shown in the sketch are used (i.e., the flux trap is contained in location D5). Also, when referring to the four large control blades, the blades are numbered consecutively starting in the lower left region of Fig. 1 and increasing in a clockwise direction. Thus, Blade 1 is in the lower left, Blade 3 in the upper right, etc., as viewed from the perspective of Fig. 1.

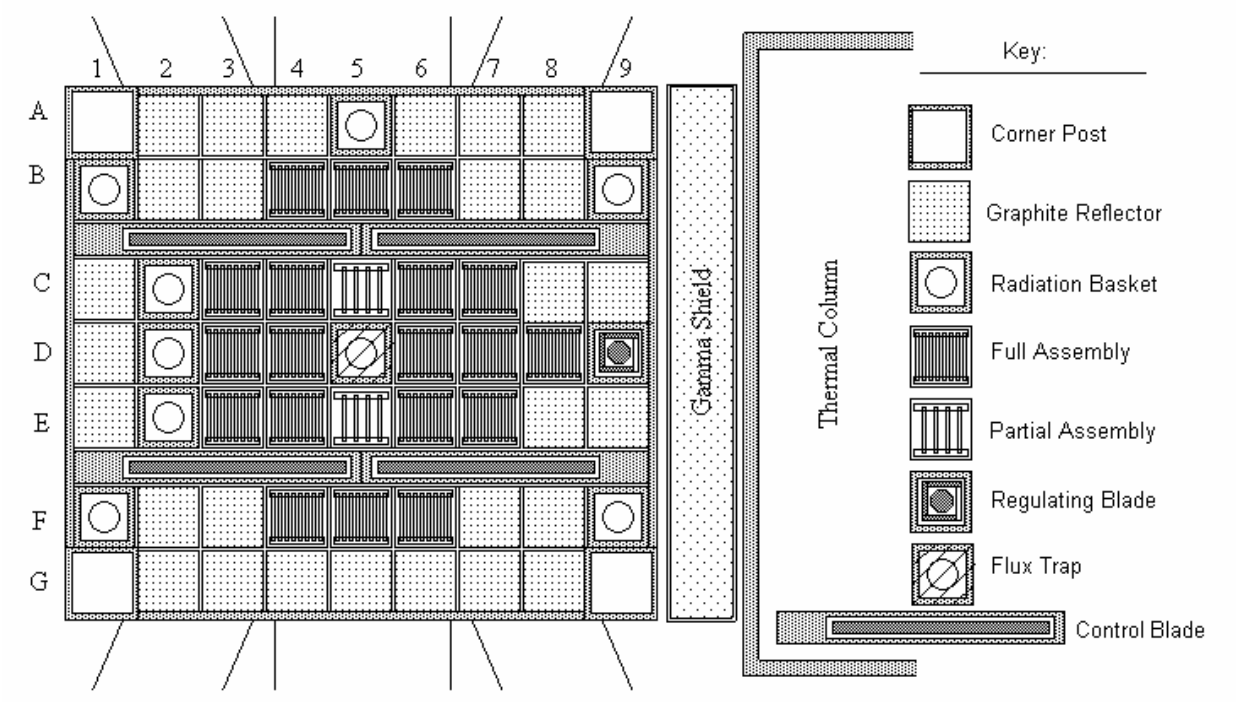

Fig. 1 Rough sketch of the LEU startup core configuration for the UMLRR (M-1-3 core).

During startup testing in Fall 2000, a series of reactivity evaluations and flux profile measurements were taken within the beginning-of-life (BOL) M-1-3 configuration to support routine operation of the new LEU core. Now, 10+ years later, these results are still important since they can be used to help validate any new models that may be developed for the UMLRR -- and this is certainly our intent here with the new MCNP models generated as part of this work.

In the latter part of 2001, a new ex-core fast neutron irradiation facility was installed within the UMLRR pool (see Refs. 9 and 10 for details). The purpose of this new experimental facility is to provide a large-volume irradiation location that has a relatively high fast neutron flux, with correspondingly low thermal neutron and gamma fluence rates. The fast neutron irradiator (FNI) replaced the three beam ports on the far side of the core (next to row A of the core grid structure). The FNI was purposely placed outside the core region for relatively easy access to the large experimental location and to minimize any effect on core operation during use of the new facility. The new irradiation facility did, however, require some changes to the actual in-core assembly configuration -- to optimize performance of the FNI and to counter reactivity effects caused by the composite facility changes. In particular, three key changes were made, including movement of the source holder from grid position A5 to G5, movement of the partial fuel elements from C5 and E5 to C3 and E3, and replacement of five graphite reflectors in row A with newly-designed lead-void assemblies (these elements eliminate the fast neutron moderation associated with graphite and they provide a first level of gamma shielding for the FNI). The resulting configuration, including the FNI grid and shield blocks, is referred to as the M-2-5 configuration and this is also the current operating layout for the UMLRR (in September 2011). This post-FNI configuration is sketched in Fig. 2.

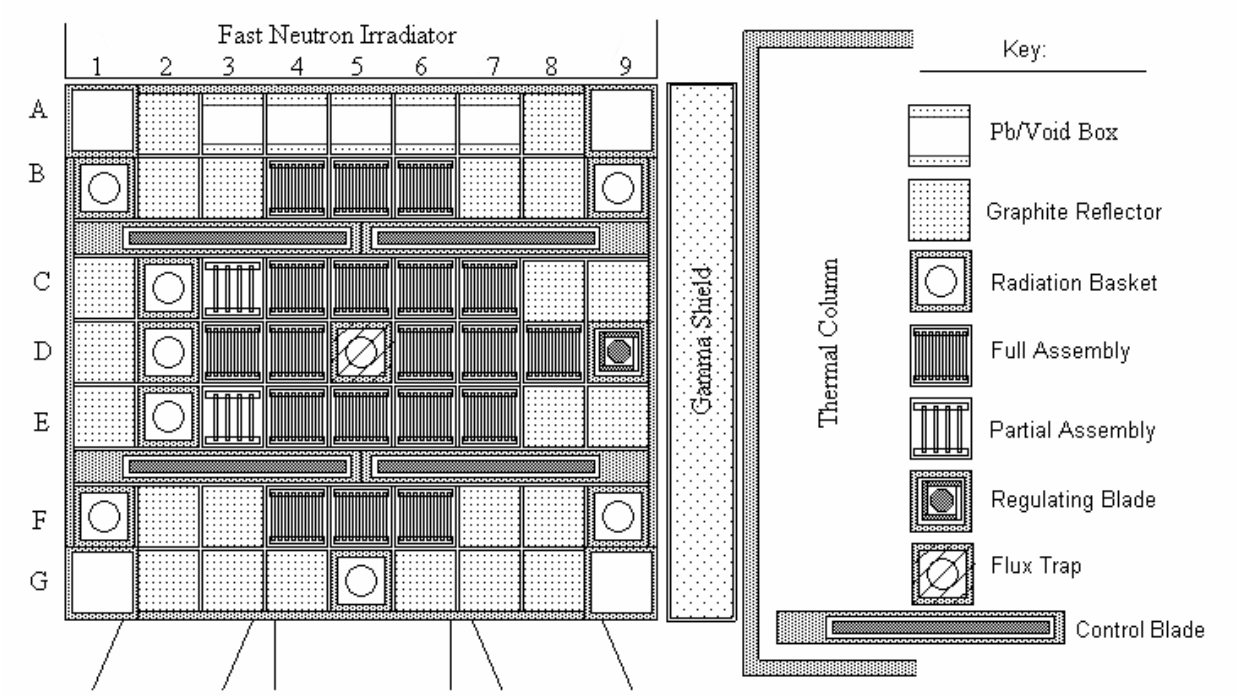

Fig. 2 Rough sketch of the post-FNI configuration for the UMLRR (M-2-5 core).

Also of note is that, during the approximately 11-year period since startup (Aug. 2000 through June 2011), the LEU core has about 1100 MWhr of total burnup (i.e. equivalent to about 46 full power days at 1 MW operation) -- where we note that the operation of the UMLRR is usually very intermittent and much of it occurs at low power in increments of only a few hours for a variety of training and educational purposes. In addition, the M-1-3 core had less than 4 MWD of burnup when the new M-2-5 configuration was installed. Thus, most of the full operating history to date has been associated with a single core layout -- that is, the M-2-5 configuration.

From a model validation perspective, the BOL M-1-3 model represents a fresh core and it has the most measured data available (reactivity evaluations and some thermal flux mappings) to support model evaluation -- thus, this configuration is the easiest and best to use for initial model validation. Next in line for model evaluation is the initial M-2-5 configuration, but only reactivity evaluations (i.e. measured blade worth curves) are available for this configuration. However, because of the low burnup level (less than 4 MWD), approximating this configuration with fresh fuel densities gives a fairly reasonable representation of reality. In contrast, for the current configuration with its nearly 50 MWD cumulative burnup, fuel depletion calculations are required to achieve a reasonable representation of the core physics. But, since the MCNP model after 50 MWD of burnup essentially represents current operations, this also creates an opportunity to perform additional measurements within the reactor to evaluate the overall suitability of the various modeling approximations. In particular, selected reactivity worths measurements associated with various bayonet insertions have been made and compared to predictions from the MCNP 3-D model. These comparisons simply give additional measured data for the current core configuration (in addition to the measured blade worth curves).

At this point, our UMLRR MCNP modeling effort is essentially complete. The three configurations noted above have been fully modeled -- that is, the M-1-3 LEU startup core, a BOL representation of the M-2-5 core, and a reasonable approximation to the July 2011 M-2-5 core with nearly 50 MWD of burnup -- and comparisons to the measured data noted above have been performed. The detailed geometry models for these cases have been discussed in previous progress reports (Refs. 1-4) and this discussion will not be repeated here. Instead, summarized below are the main results of the validation study which show, without doubt, that we were indeed successful in generating a series of MCNP models that accurately predict the behavior of the actual UMLRR system. There are four primary comparisons made as part of the validation effort, as follows:

1. Prediction of the "critical" k_{eff} for each of the three critical configurations.
2. Comparison of the computed and measured total worths for each of the five control blades for each configuration. Also of interest here is an estimate of the excess reactivity for each configuration.
3. Comparison of some selected axial thermal flux profiles from MCNP and measured data for the M-1-3 core. Note that an experimental program to measure the axial thermal flux profiles in selected irradiation positions for the current M-2-5 configuration is underway, but this effort is outside the scope of the current project and these measurements will not be discussed further in this report. Data from these additional evaluation tests will be published as part of a student thesis at a later time.
4. Comparison of some selected reactivity worth measurements within the initial M-1-3 startup core and in the current M-2-5 configuration with nearly 50 MWD of burnup.

Each of these comparisons will be discussed separately in the following pages.

Prediction of the "critical" k_{eff} : The critical configurations for the M-1-3 startup core, the M-2-5 BOL core, and the July 2011 M-2-5 core with nearly 50 MWD of burnup, all give good results for the "critical" reactivity level of the system, as summarized in Table 1. Note that two M-2-5 BOL models were generated, including the reference model with a simple fuel zone description and a more complex depletion-ready model with 105 separate fuel zones within the model (however, all the zones had the same material composition for the BOL state). Clearly Table 1 shows that both the reference and depletion-ready BOL M-2-5 models give essentially the same result -- as they should. Overall the predicted critical k_{eff} values were very close to unity for all the cases, indicating that the final MCNP models can predict the absolute reactivity level of the UMLRR with good accuracy (see Ref. 4 for a discussion of how the preliminary results were improved by changing the initial control blade model and by measuring the graphite density within the UMLRR system).

Table 1 Summary results for several critical configurations within the UMLRR.

Model Description	Blades 1-4 Location (inches out)	Regulating Blade Location (inches out)	Computed "Critical" K_{eff}	Standard Deviation (20M histories)
BOL M-1-3	15.3	8.0	0.99498	0.00017
BOL M-2-5	14.9	10.0	0.99869	0.00018
BOL M-2-5 (depletion ready)	14.9	10.0	0.99838	0.00017
M-2-5 at 50 MWD	16.3	7.7	0.99563	0.00017

Prediction of the Blade Worth Curves: Estimating the reactivity worth associated with each of the four large control blades and the low-worth regulating blade within the UMLRR was another main component of the MCNP model evaluation process. The blade worth curves within the system must be measured on an annual basis at a minimum, and this is also one of the first measurements made each time a substantially new critical core configuration is established. Thus, measured data are available for all three core configurations modeled as part of this work. Unfortunately, however, the discussion of the blade worth results is quite cumbersome for several reasons -- mostly because of the large amount of uncertainty that exists in the resultant "measured" curves (see the discussion below). In addition, the $\Delta k/k$ data from the discrete MCNP ***kcode*** calculations also contain inherent statistical uncertainty, with a maximum standard deviation as high as 10-15 $\%\Delta k/k$ at the endpoints of the blade traverse. Thus, the comparisons here are not as "clean" as desired and are more qualitative in nature than quantitative -- with focus on obtaining the proper blade worth distribution among the four blades, along with a reasonable estimate of the absolute magnitude of the total worth of each blade.

The basic approach for measuring the desired worth curves within the UMLRR involves the measurement of the reactivity induced due to a small movement of a blade. For example, a blade that is suddenly withdrawn a small amount translates to a positive reactivity addition, which causes a critical system to go slightly supercritical. This results in an increase in power and, after a short transient time to allow the reactor to reach a stable positive period, one can easily measure the doubling time and convert this to reactor period, τ, using the 6-delayed group reactivity equation. After each discrete movement of a test blade, the midpoint of the motion is recorded along with the associated change in reactivity that occurred due to the imposed change in blade height, Δz. Several

of these differential worth measurements are made, fit to a mathematical model, and then integrated to give the desired integral worth curves for each of the blades within the UMLRR.

Unfortunately, the reactor staff have routinely used a simple cosine model to do the curve fits (see Ref. 11, for example, for a typical blade worth curve). However, this pure theoretical approach assumes a symmetric axial worth distribution -- which is not valid within the UMLRR since, during normal operation, the blades are usually inserted 8 – 11 inches into the top of the core. This situation leads to a bottom peaked flux and differential worth profile, especially at BOL when the blades are inserted the most. Several years ago (see Ref. 5), an alternative cubic polynomial + cosine model was proposed, and this has been shown to give significantly better curve fits if a sufficient number of data points evenly spaced over the full 26″ range of the blades is available. Here we will show some example results using both curve fit models to illustrate the type of differences that are typically observed -- however, it should be emphasized that, if the above conditions are met (i.e. sufficient coverage of the experimental data), the cubic polynomial + cosine model generally is a much better choice. This is not always possible, however, which is one reason why the reactor staff continue to use the simple symmetric model. Unfortunately, neither approach is ideal in all cases, and this situation complicates the issue of obtaining accurate blade worth curves (although the polynomial + cosine model is often the better choice).

As an illustration of the above issues, the measured blade worth results from the startup test program for the M-1-3 core are summarized in Table 2. As noted above, the "theoretical model" refers to a symmetric cosine-only differential blade worth curve and the "new model" represents a 3^{rd}-order polynomial + cosine model for fitting the differential worth data. The measured critical height had Blades 1 – 4 banked at 15.3 inches withdrawn with the regulating blade at 8 inches out. The tabulated excess reactivity is the remaining worth associated with the movable blade length above the critical height (full out is about 26 inches withdrawn).

Table 2 Measured results from M-1-3 startup core (August 2000).

	Theoretical Model (simple cosine fit)			**New Model (3^{rd} order polynomial + cosine fit)**		
Blade #	**Total Worth % Δk/k**	**Fit Quality R^2 Value**	**Excess Reactivity % Δk/k**	**Total Worth % Δk/k**	**Fit Quality R^2 Value**	**Excess Reactivity % Δk/k**
Blade 1	2.53	0.90	0.83	2.63	0.98	0.66
Blade 2	2.38	0.78	0.78	2.47	0.90	0.57
Blade 3	3.34	0.89	1.09	3.32	0.96	0.80
Blade 4	3.19	0.83	1.04	3.20	0.91	0.79
Total Worth Blades 1 – 4	11.4	--	3.74	11.6	--	2.82
Regulating Blade	0.28	--	0.23	--	--	--

Because of the low total worth, only two experimental data points were taken for the regulating blade. Therefore, the new model could not be used with the limited experimental data available for the regulating blade (need a minimum of 5 data points).

Concerning the curve fits, there is a fair amount of experimental uncertainty in the raw differential worth data, especially for Blades 2 and 4 -- as apparent from visual inspection of the curve fits (see Fig. 3 below for the Blade 2 data, for example) and via the R^2 correlation coefficient noted in the above table. Also, in all cases, the new model gives significantly better fits relative to the theoretical model due mainly to the real asymmetric nature of the measured data. The difference in the two models, forced symmetry for the theoretical model versus potential asymmetry within the new model, also accounts for part of the difference in the prediction of the total excess reactivity for the UMLRR M-1-3 startup core. However, the poor comparison for the excess reactivity values is mostly due to the overall poor curve fits (that are due to the large variation in the measured data as illustrated in Fig. 3). Thus, neither excess reactivity value is overly reliable, but it is expected that the real excess reactivity in the LEU startup core was closer to 4% Δk/k than to the 3% Δk/k value (as observed from operational experience). Overall, however, it is clear that the experimental data are rather imprecise, so the total worths and excess reactivity values can only be treated as approximate values. In general, the polynomial + cosine model gives the best fits but, even here, with some R^2 values around 0.90, these are not considered very good fits to the data.

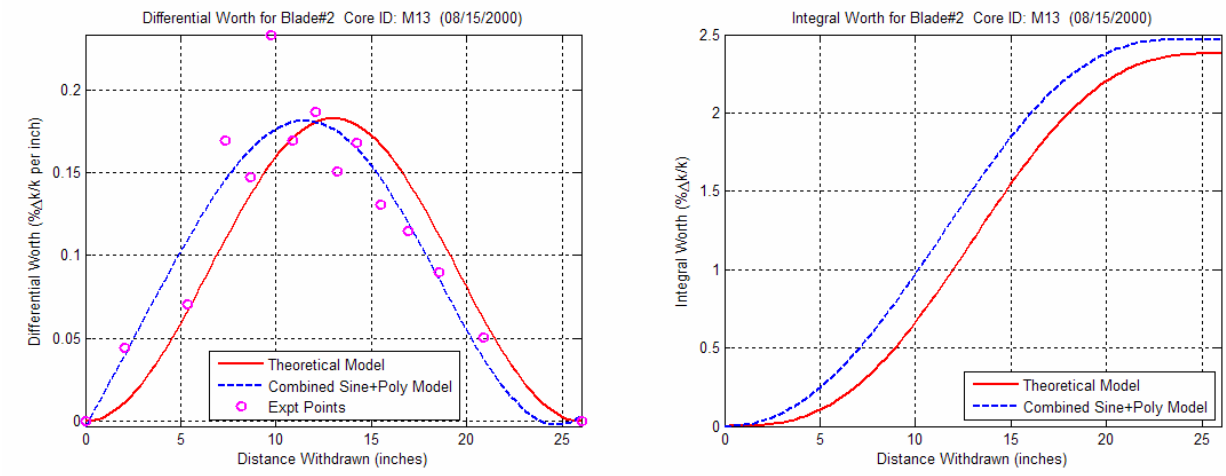

Fig. 3 Typical example of the raw measured data and resultant curve fits for the differential and integral blade worth curves (Blade 2 in M-1-3 core).

Note that the experimental approach for determining the blade worth curves can be easily simulated with the 3-D MCNP model by simply doing a series of k_{eff} calculations with the blades at different heights. In practice, the MCNP blade worth calculations were done with the goal of keeping the reactor roughly "near critical" (which in this case was k = 0.995 ±0.005). Thus, the remaining blades were rebanked at various stages, as needed, to maintain a near critical configuration at each step in the process. The k_{eff} values and blade locations were then used to compute the differential worth estimates and to generate the blade worth curves using only the MCNP-computed values.

The simulated blade worth data obtained from the MCNP M-1-3 BOL model are summarized in Table 3. The data shown here should be compared to the measured results given in Table 2. In general, the blade worth predictions from the 3-D MCNP model agree reasonably well with the

measured data, but they are generally a little on the high side. One important factor to consider, however, is that there is much less variability in the simulated raw data, which gives better overall curve fits (i.e. compare the R^2 values from the tables and the simulated Blade 2 worth curves in Fig. 4 versus the measured data in Fig. 3). This behavior is typical for all the blade worth data generated in this study.

Table 3 Computed results for M-1-3 startup core using the August 2011 MCNP model.

	Theoretical Model (simple cosine fit)			New Model (3^{rd} order polynomial + cosine fit)		
Blade #	**Total Worth % Δk/k**	**Fit Quality R^2 Value**	**Excess Reactivity % Δk/k**	**Total Worth % Δk/k**	**Fit Quality R^2 Value**	**Excess Reactivity % Δk/k**
Blade 1	2.82	0.87	0.92	3.00	0.97	0.79
Blade 2	2.62	0.92	0.86	2.75	0.98	0.75
Blade 3	3.22	0.91	1.06	3.42	0.99	0.93
Blade 4	3.37	0.89	1.10	3.55	0.96	0.97
Total Worth Blades 1 – 4	12.0	--	3.94	12.7	--	3.44
Regulating Blade	0.32	0.63	0.27	0.38	0.98	0.25

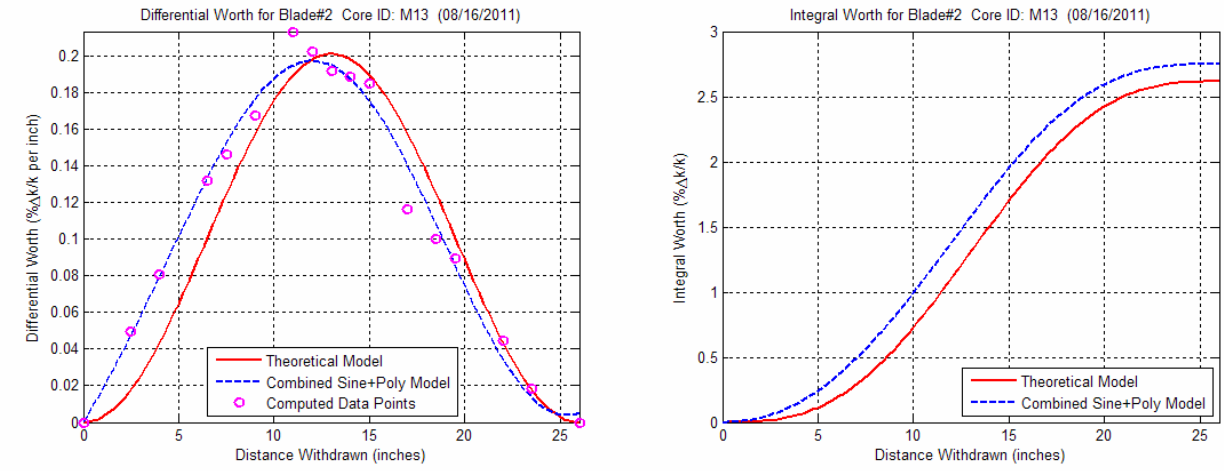

Fig. 4 Typical example of the raw data from the 3-D MCNP calculations and the resultant curve fits for the differential and integral blade worth curves (Blade 2 in M-1-3 core).

The MCNP model generally used 20 million histories (10000 particles per cycle with 2000 cycles) after the fission source had converged to generate the nominal k_{eff} for each different blade configuration. This number of histories resulted in a standard deviation of about 0.017% $\Delta k/k$ for each case. This uncertainty, although small for the estimate of k_{eff}, actually leads to a nontrivial uncertainty in the predicted $\Delta k/k$ values for each step (the computed $\Delta k/k$ values ranged roughly between 0.2 and 1.0% for the four large control blades, except at the endpoints of the blade traverse). Thus, the statistical uncertainty was generally much less that ±10-12% for an individual differential worth point (again, except for the top endpoint near z = 26 inches withdrawn). For these calculations, the uncertainty in Δk was obtained as the square root of the sum of the squares of the individual errors (i.e., $\sqrt{0.017^2 + 0.017^2} \approx 0.024$) and the maximum relative error is this value divided by the smallest $\Delta k/k$ used -- which gives roughly 0.024/0.2 = 0.12. Thus, the MCNP uncertainty was generally lower than the measurement uncertainty (as seen graphically in Figs. 3 and 4) so, even with the inherent statistical error, the MCNP-computed results were indeed quite acceptable for comparison purposes.

For the low worth regulating blade, however, a minimum of 50 million histories were needed as well as relatively large Δz increments to keep the statistical uncertainties to reasonable values (some cases were actually run with 100 million histories). For this blade, the $\Delta k/k$ values were generally around 0.10 to 0.15% and the 1σ value for each k_{eff} calculation was about 0.011% $\Delta k/k$ for the 50 M history cases -- thus, most of the individual differential worth points had uncertainties around ±10-12%, whereas, for the large shutdown blades, this was the maximum uncertainty. However, even with the somewhat higher inherent statistical uncertainty, the curve fit for the new model was quite good for this case (recall that there were only two measured points for the regulating blade, so that the enhanced curve fit model could not even be used with the actual experimental data). Finally, within this context, we should note that the quality of fit for the regulating blade worths tend to be quite different for the symmetric theoretical model vs. the asymmetric curve fits, because the four large control blade are inserted to their largest operating depth when computing the regulating blade worths (about 15.3″ withdrawn) -- and this leads to the largest actual asymmetry that is observed in the differential blade worth curves.

Well, to summarize the above discussion, it is clear that there is inherent uncertainty in both the measured and MCNP-computed blade worths, with the MCNP uncertainty generally lower than or on par with the experimental uncertainty. In addition, when sufficient data are available, the cubic polynomial + cosine model generally does a much better job at matching the trend in the bottom-peaked discrete differential worth data. Thus, for the remaining configurations, only the data for the "new model" is given (where possible), since this represents the best estimate of the true reactivity worth.

The same type of calculations and measurements as discussed above were completed for all three UMLRR configurations and a complete set of the computed vs. measured total blade worths and the total core excess reactivity are summarized in Table 4. In addition, a totally independent method for directly measuring the integral blade worth curve using inverse kinetics is currently being developed at UMass-Lowell for use within the UMLRR. This work is not complete and has not been published as yet -- however, preliminary estimates of the total blade worths for the M-2-5 core from March 2011 using this new methodology are available, and these have been included in the last column of Table 4 as an independent estimate of the measured worths for this configuration.

Table 4 Computed vs. measured blade worth results for all three UMLRR configurations (the curve fits use the cubic polynomial + cosine model except where noted with an asterisk).

	M-1-3 BOL Core Total Worth (% Δk/k)		M-2-5 BOL Core Total Worth (% Δk/k)		M-2-5 at 50 MWD Total Worth (% Δk/k)		
Blade #	**Measured**	**MCNP**	**Measured**	**MCNP**	**Measured**	**MCNP**	**Inverse Kinetics**
Blade 1	2.63	3.00	2.82	2.76	2.55	2.73	2.66
Blade 2	2.47	2.75	2.19	2.40	2.23	2.40	2.23
Blade 3	3.32	3.42	3.19	3.42	3.64	3.19	3.34
Blade 4	3.20	3.55	3.93	3.83	4.19	3.71	3.64
Total Worth Blades 1 – 4	11.6	12.7	12.1	12.4	12.6	12.1	11.9
Excess Reactivity Blades 1 – 4	2.82	3.44	3.46	3.46	2.41	2.60	--
Regulating Blade	0.28*	0.38	0.30*	0.38	0.31	0.38	0.31

Generally good agreement to within 10-15% is apparent for most of the MCNP vs. experimental results -- and, considering the observed uncertainty in both methods, this is actually quite good. In addition, all the expected trends are predicted quite nicely with the various MCNP models. For example, the fuel and graphite/water reflector arrangement suggests that, for the M-1-3 BOL core, there should be a slight tilt in the flux and blade worth distribution in the direction of Blades 1 and 4, with an additional slight shift towards Blade 4 (lower right portion of Fig. 1). Thus, for the BOL M-1-3 core, we would expect the worths for Blades 1 and 2 to be comparable, with Blade 1 worth a little more than Blade 2. Similarly, Blades 3 and 4 should have comparable worths, with Blade 4 having the largest reactivity effect of all the blades. For the M-2-5 configurations, the basic worth distribution is expected to be the same, but the asymmetry should be magnified significantly because of the movement of the partial assemblies to the left side of the core (Column 3 instead of Column 5) and the replacement of five graphite reflectors in Row A with Pb-void elements. Thus, for this configuration, Blade 2 is expected to have the lowest worth and Blade 4 the highest, with the difference being much larger than for the M-1-3 layout. These expected trends are exactly as observed in Table 4, which gives good confidence in the overall ability of the MCNP models to predict these effects.

Concerning the regulating blade worths, the MCNP values are consistently high by 20-25% relative to the measured values (but the absolute differences are rather small). Based on our experience to date with these analyses, we initially had more confidence in the computed values than the experimental values because of the small number of experimental points used and the resulting uncertainty in the measured result. However, the independent inverse kinetics method, which uses many more data points collected over a short transient run, tends to support the lower regulating blade worths determined from the doubling time experiments. Thus, this suggests that the regulating blade worth may indeed be closer to 0.31 than 0.38% Δk/k -- but the jury is still out here…

Axial Thermal Flux Profiles in the M-1-3 Core: A combination of gold foils and copper wires were used to perform thermal flux mapping in selected locations of the M-1-3 LEU startup core as illustrated in Fig. 5. Cadmium-covered and bare gold foils were used to provide an absolute determination of neutron fluence rate, while copper wires provided an axial flux distribution at the chosen locations. The gold foils and some comparison copper wires were installed near the axial midpoint of two standard sample bayonets and then lowered into the radiation baskets in grid locations C2 and E2. Five long copper flux wires (nearly 3 feet long in some cases) were placed between the fuel plates of un-irradiated fuel elements in positions D6 and E6 and into the D2 and D5 irradiation positions as shown. The wire was held in place in the center of the D5 location using suitable spacers within a sample bayonet. All the bayonets in the core (positions C2, E2, and D5) were flooded. The irradiations were then performed at an indicated power level of 100 watts for 30 minutes.

After irradiation, the wires and foils were removed and counted on a gamma spectrometer. An inter-calibration between the gold foils and copper wires provided an absolute flux distribution at the five wire locations indicated in Fig. 5. All the measured flux distribution data were then normalized to a nominal power level of 1 MW and compared to the results from the MCNP computational model for the M-1-3 core with the four large control blades positioned at 15.3 inches withdrawn and the regulating blade at 8 inches out.

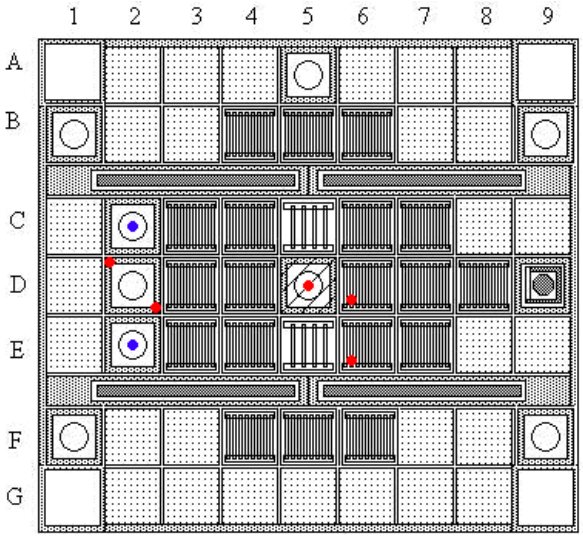

Fig. 5 Location of the gold foils (blue) and copper wires (red) for the flux mapping measurements.

Summary results from these comparisons are shown in Fig. 6. The individual small circles on these curves represent the experimental values of the absolute thermal flux and the dots with the 1σ error bars are associated with the MCNP results. The top two plots highlight the two copper wires in the D2 position, with relatively good agreement in both cases. In particular, the MCNP thermal flux profile in the upper left D2 location gives a near perfect match with the measured profile and, for the lower right wire in D2, the worst case difference in the peak fluxes is only in the 10-12% range.

The results for the wires in the two fuel assemblies are shown in the middle plots in Fig. 6. The particular locations for the wires in the D6 and E6 fuel assemblies were chosen because these were near the locations of the peak power density as determined from the preliminary design calculations.

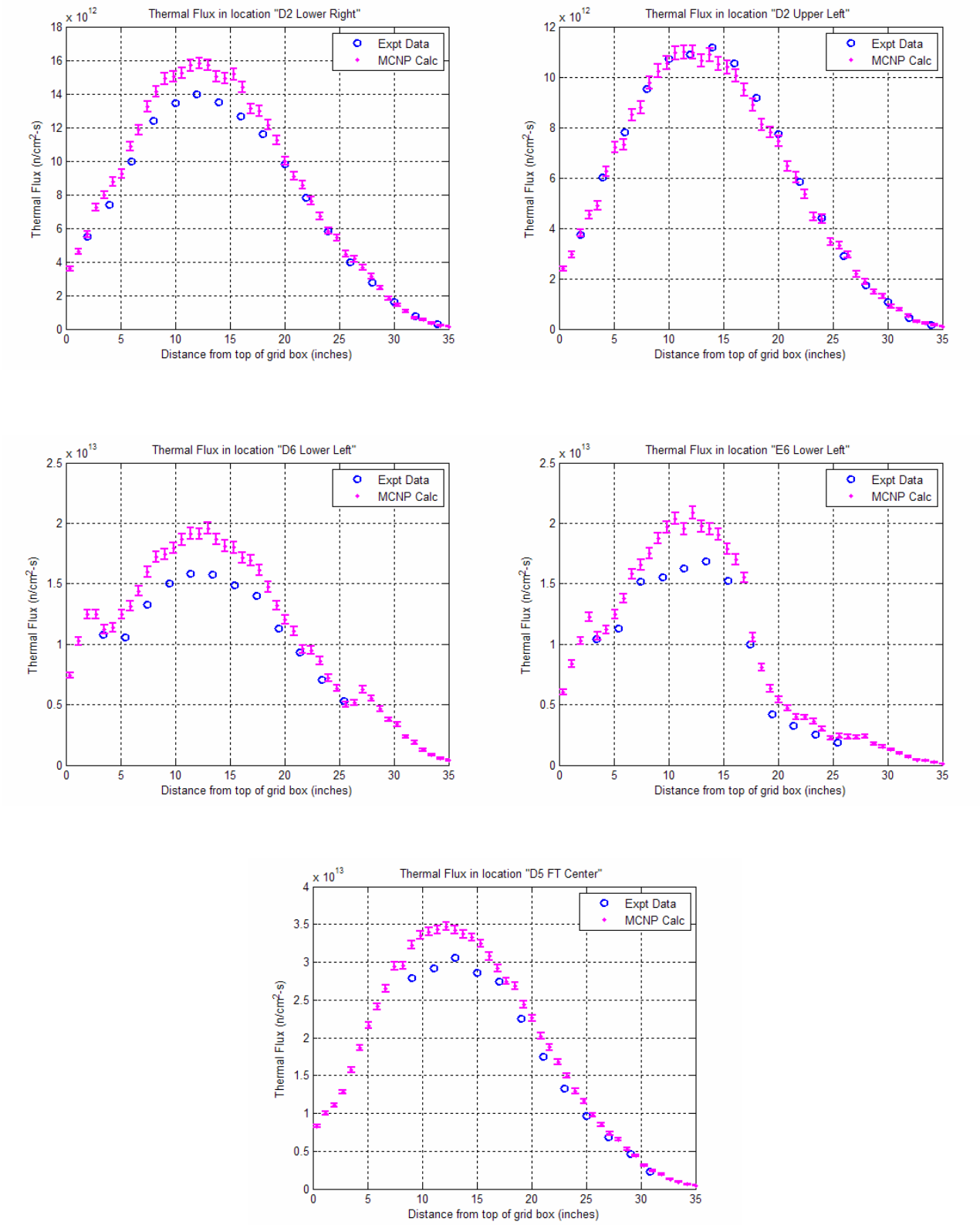

Fig. 6 Calculated vs. measured axial thermal flux profiles at various locations (M-1-3).

As apparent, the MCNP simulation over-predicts the thermal flux in these regions by as much as 20-25%. However, the basic axial thermal flux distributions are as expected. For example, since the copper wire in E6 is very close to Blade #4 which is inserted to a depth of about 15.3+2.5 = 17.8 inches above the grid box, one would expect a large flux gradient in this area, and both the calculations and measurements show this quite clearly. In addition, we note that the LEU fuel assembly height is 30 inches, with 23.5 inches of fuel meat and 3.25 inches of aluminum structure and water just above and below the active fuel region. Although there are limited experimental data to validate the computed profile, the MCNP calculations clearly show the expected thermal flux peak near the top and bottom fuel/reflector interfaces. Thus, the computed flux profiles are quite reasonable, although the flux level is a little high relative to the experimental data.

The bottom curve in Fig. 6 shows the computed and measured thermal flux profiles in the center of the flux trap assembly in location D5. The agreement here is also quite reasonable, with a good representation of the axial shape and a slight over-prediction of the flux magnitude by roughly 10-15%. This experimental location has the highest thermal flux magnitude within the UMLRR and this irradiation position is used whenever high fluence or fluence rates are needed.

Finally, we should note that there is not a lot of information available about the uncertainty in the experimental measurements that were taken back in August 2000 (only nominal flux values are available). This is unfortunate, since it is difficult to draw quantitative conclusions about the accuracy of the MCNP model without some idea as to the accuracy of the experimental data. One concern, for example, is that the measurements were performed at a power level of approximately 100 W and the measured data were then scaled to 1 MW -- thus, even a small error in this "approximate" power level could account for a magnitude difference in the measured and computed results. Overall, however, the five experimental and MCNP-computed axial profiles show the same qualitative behavior and the magnitudes agree reasonably well, with the MCNP values generally on the higher side by roughly 10-25% (except for the upper left D2 location which was "right on target").

Note: New flux profile experiments are planned for the current M-2-5 core configuration so that we can get a comparison of the 50-MWD MCNP model relative to measured data, and to also address the expected uncertainty in the actual measured profiles. However, this work is outside the original scope of this project and summary results will not be available until late Fall 2011. These comparisons will be part of a student thesis, and the full thesis document will be generally available soon after formal publication in early 2012.

Selected Reactivity Worth Comparisons: As a final indicator of the general reliability of the UMLRR MCNP models, we have also compared a number of measured reactivity worth results with those computed using the MCNP models for the BOL M-1-3 core and for the M-2-5 configuration after nearly 50 MWD burnup. In particular, Table 5 summarizes a series of reactivity worth tests that were available for comparison to the MCNP-computed results. The majority of the tests involve the insertion of an empty (air-filled) bayonet into one or more specific locations. However, one test in the M-1-3 core also measured the worth of a water-filled bayonet in the flux trap. Finally, we also recently determined the worth associated with the replacement of a burnt fuel element in location D6 with a fresh uranium-silicide assembly.

Note that, in these comparisons, it is important to emphasize that the 1σ uncertainty in the MCNP computations is about 0.02% $\Delta k/k$ (some were about 0.017% and others were about 0.022%), and this is a very large uncertainty when the absolute actual $\Delta k/k$ is less than 0.1%. In addition, as noted above, there is also a fair amount of uncertainty in the blade worth curves which were used to get

the “measured” reactivity worths. Thus, the best we can hope for here with these small worth measurements is to be “in the ballpark” with the correct sign (positive or negative) for the reactivity change. For the larger worths, however, a more quantitative comparison is possible.

Table 5 Computed vs. measured reactivity worth results for selected configurations.

Case #	Description of Experimental Configuration	M-1-3 BOL Core Reactivity Worths (% Δk/k)		M-2-5 at 50 MWD Reactivity Worths (% Δk/k)	
		Measured	MCNP	Measured	MCNP
1	air-filled bayonet in flux trap (D5)	0.25	0.20	0.11	0.14
2	water-filled bayonet in flux trap (D5)	0.03	0.06	--	--
3	air-filled bayonet in radiation basket (D2)	-0.01	-0.07	--	-0.05
4	air-filled bayonet in radiation basket (C2)	--	--	-0.00	-0.02
5	air-filled bayonets in both C2 and D2	--	--	-0.02	-0.08
6	air-filled bayonets in C2, D2, and E2	--	--	-0.02	-0.08
7	interchange fresh fuel assembly with the burnt fuel element in D6	--	--	0.10	0.10

Well, as apparent from Table 5, the measured and calculated reactivity worths are indeed “in the ballpark”. In general, small measured reactivities map to small computed values and the correct direction of the change is consistently predicted. For the larger changes, as apparent for Case 1 for example, the magnitude of the change is also well predicted within our uncertainty constraints. Here, it should be noted that the UMLRR has an over-moderated assembly design -- thus, removal of moderator from the central core region gives a positive reactivity effect. On the other hand, in the basket locations on the core periphery, the increase in void associated with the bayonet insertion also leads to increased leakage, which more than offsets the positive contribution due to the over-moderated assembly design -- thus producing a small net reduction in reactivity.

For Case 7, it was estimated that the burnup associated with the fuel element in location D6 was approximately 2.75 MWD, which gives a reduction of slightly over 3 grams of U235 relative to a standard fresh fuel assembly. Thus, by replacing this burnt element with a fresh assembly, one would expect a positive reactivity addition associated with about 3 grams of fissile material near the center of the core. As apparent from Table 5, the reactivity effect was indeed positive and the predicted magnitude was right on target with the measured result.

Summary Results for the UMLRR MCNP Models: The MCNP validation effort has looked at critical blade heights, total blade worths, selected thermal flux profiles, and a limited set of reactivity worth measurements in both the M-1-3 and M-2-5 core configurations. In all cases, the MCNP results are reasonable and they consistently exhibit the expected behavior of the system. In general, the combined experimental error and the statistical uncertainty in the MCNP calculations make it difficult to perform a rigorous quantitative comparison but, with due consideration for these expected tolerances, one can argue that the MCNP models are quite representative of the real system with generally good overall agreement in all the calculated and measured results. Thus, the MCNP

models have successfully passed their first set of validation tests. Of course, model validation is a never-ending process -- so we plan to continually evaluate the real predictive capability of the MCNP models as they are used to support the analysis of subsequent experiments within the UMLRR facility.

Updated Results for the Co-60 Rack-in-Pool Experimental Arrangement

In addition to the MCNP modeling of the UMLRR, another subtask associated with this overall project involved modeling of some of the Co-60 irradiation facilities within the UMass-Lowell Radiation Laboratory. Specifically, we were tasked with the generation of two MCNP models -- one containing a standard Co-60 rack within a large water volume, and another which contains the same rack integrated with the UMLRR gamma cave geometry. The rack-in-pool model, along with some preliminary results, were described in Ref. 4 and a discussion of the gamma cave irradiation facility is described in detail (for the first time) in the next section of this report (see below). For the rack-in-pool model, however, we have generated some new information and corrected some erroneous data given in Ref. 4, and these updates are discussed in this section within the following paragraphs.

Concerning the rack-in-pool model, this is simply a standard Co-60 rack, sitting on a 1″ thick aluminum plate, in a large pool of water. The origin of the system is in the center of the rack geometry and the overall rack dimensions are approximately 9.75″ × 0.625″ × 19.1″ in the x, y, and z directions, respectively. The surrounding water region extends 3 ft on both sides of the origin in the x and z directions and, in the y direction, it extends 2 ft behind the rack and 6 ft in front of the rack.

The rack itself, as shown in the focused views given in Figs. 7 and 8, contains 18 possible pencil locations, but only 16 locations have active Co-60 pencils inserted, with the two center locations left empty to help flatten the resultant gamma flux profile in the vicinity of the rack. The outer SS316 structure secures the individual pencils in the desired locations and creates a rigid rack geometry that allows easy handling and placement of the rack in various irradiation facilities (i.e. this same rack was used for the gamma cave irradiations as well as for the rack-in-pool tests).

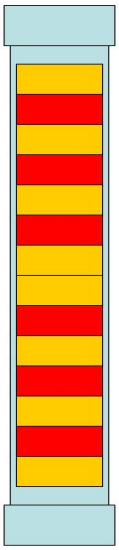

The active pencils are C-188 Co-60 sealed sources obtained from MDS Nordion Inc. (see Ref. 12). These pencils contain six active Co-60 slugs (red) and 8 inactive cobalt slugs (yellow), placed as shown in the rough sketch to the right (sketch is not to scale). Note that, since both the activated and inactive slugs are cobalt metal, the MCNP geometry in Fig. 8 does not explicitly model the layered geometry as illustrated in the sketch. However, the discrete axial placement of the gamma sources in only the active slug locations is indeed important, and this is properly treated within the MCNP source description (this will be apparent in some of the results shown below).

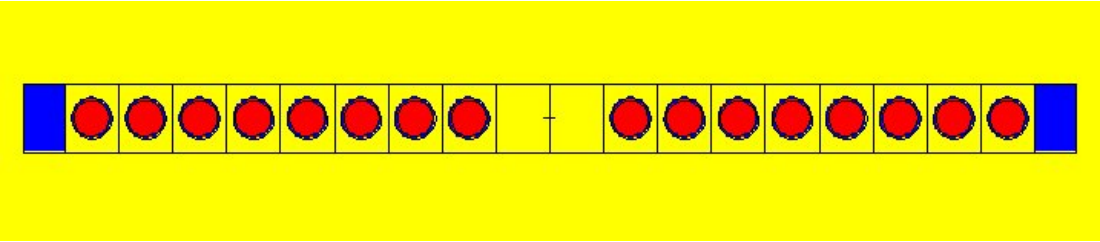

Fig. 7 Top view (xy plane) of MCNP model for the Co-60 rack (z = 0).

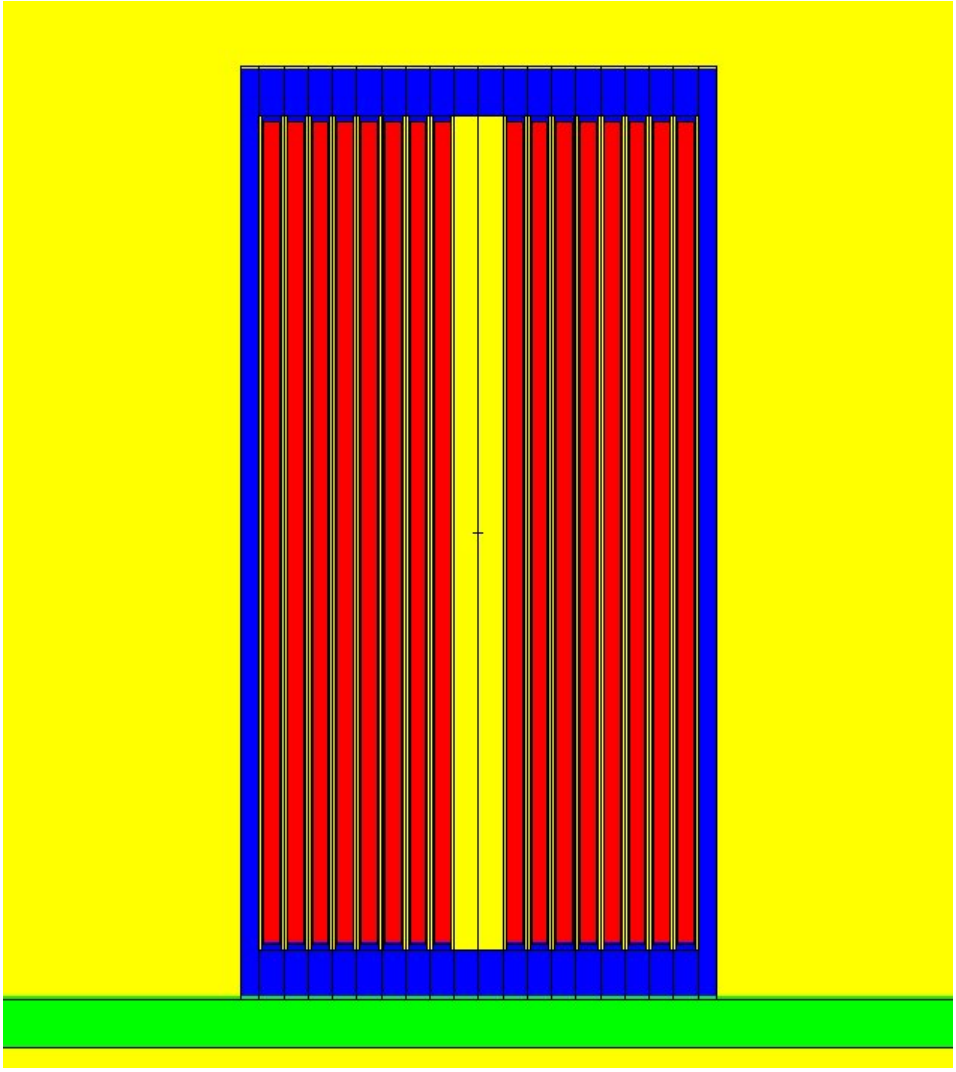

Fig. 8 Side view (xz plane) of MCNP model for the Co-60 rack (y = 0).

The total Co-60 activity of each pencil is specified when purchased from the supplier and each pencil is tagged so that its activity versus time can be tracked. The rack used in the experimental testing done in late October 2010 was Co-60 Rack C-2 and the activity level by pencil for that particular rack on that specific test date has been incorporated directly into the MCNP source specifications. The total source activity for Rack C-2 at the end of Oct. 2010 was about 19.9 kCi and this translates to a total gamma source strength of about 1.472e15 gammas/sec. This value was used to normalize the resultant gamma fluxes per source particle that is output from MCNP to give an absolute flux level in particles/cm^2-sec.

Concerning results, the primary quantity of interest here is the total gamma flux as a function of position from the rack center, with focus on its attenuation versus distance in the +y direction. To obtain this information, an MCNP ***fmesh*** tally over a 3-D rectangular grid surrounding the rack was obtained and processed/plotted within a short Matlab code. In particular, the ***fmesh*** tally results over a 2 cm grid are displayed in Figs. 9 – 12 in a variety of formats (see **Note** below).

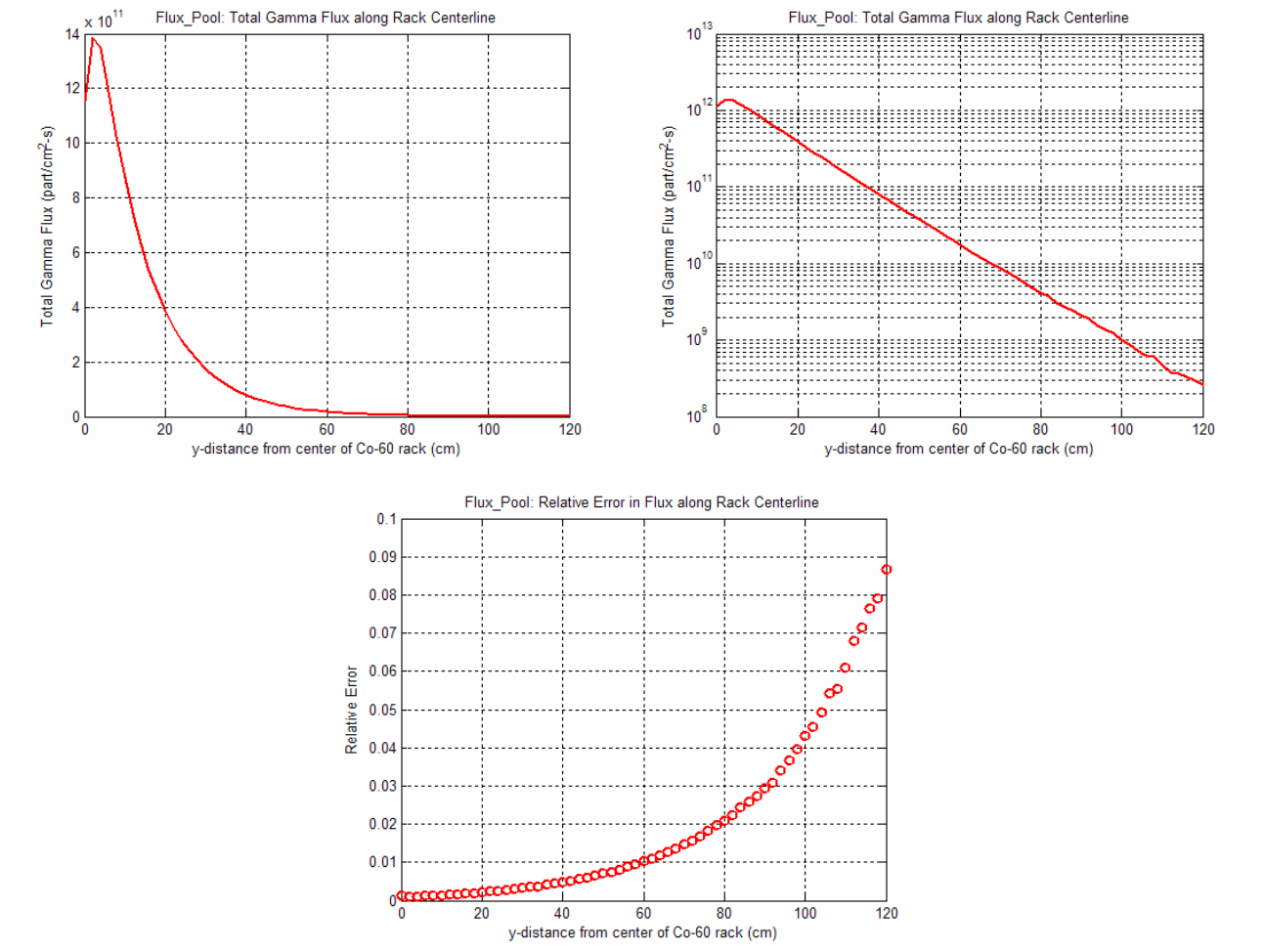

Fig. 9 Gamma flux and fractional error vs. y along the rack centerline.

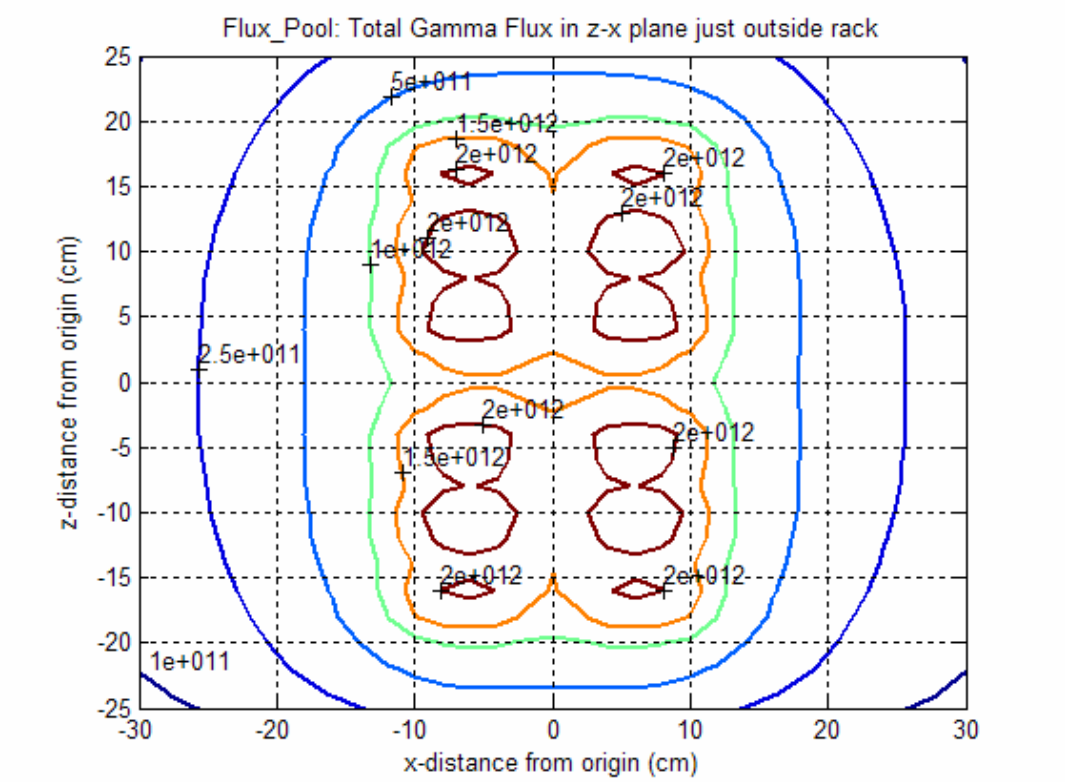

Fig. 10 Gamma flux distribution in the xz plane just outside the source region.

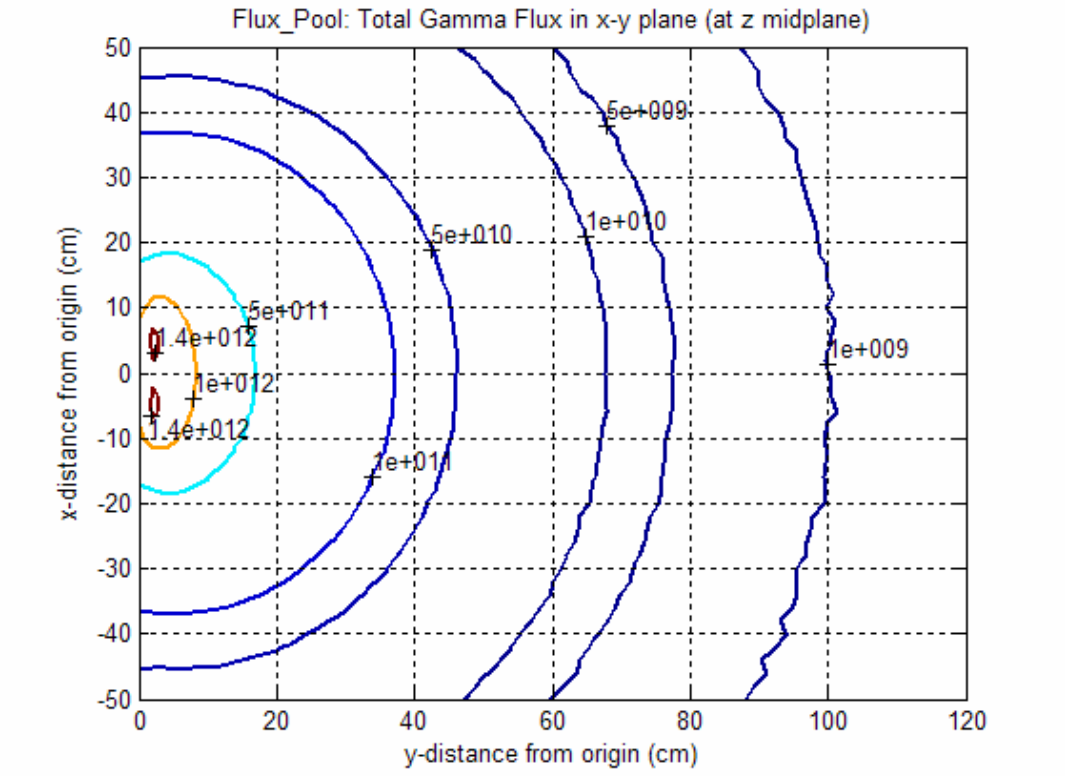

Fig. 11 Gamma flux distribution in the xy plane at z = 0.

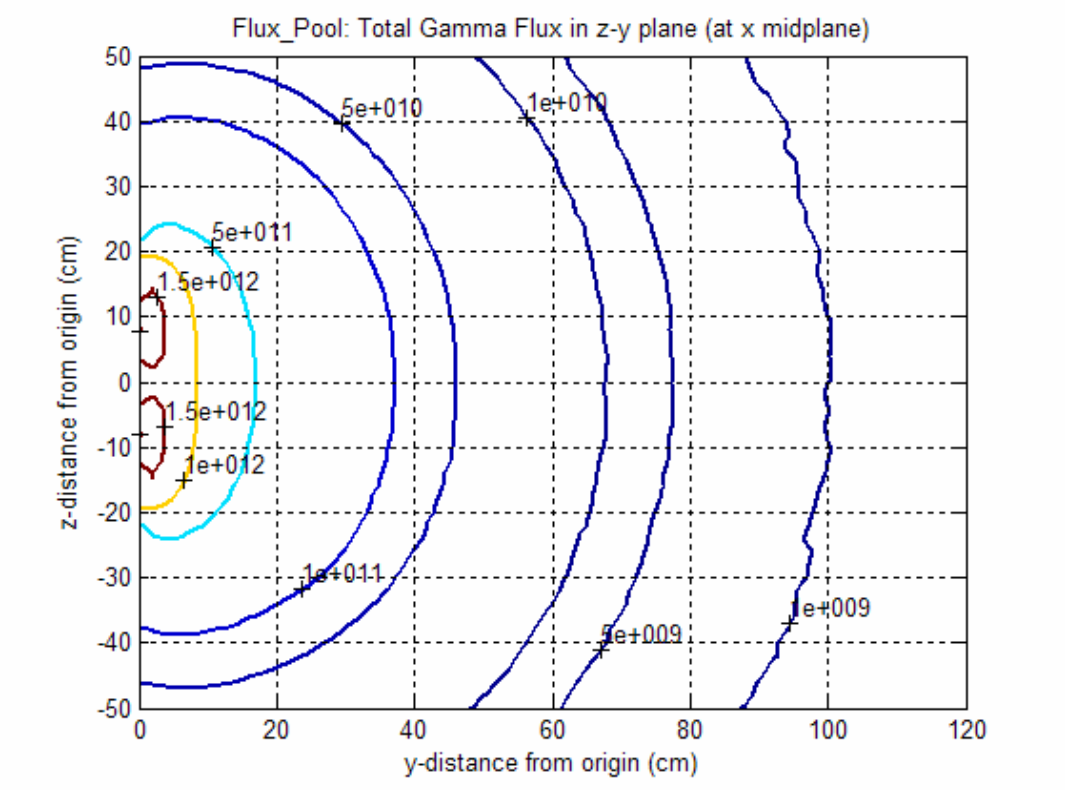

Fig. 12 Gamma flux distribution in the zy plane at x = 0.

Note: Similar preliminary gamma flux data using a somewhat coarser mesh were previously displayed in Ref. 4, but those results incorrectly referenced the wrong mesh entries -- thus, the data presented in Ref. 4 do not reflect accurate centerline values. The results presented in this Final Report have a finer mesh structure and the proper centerline mesh values have been selected. In addition, the surface plots from Ref. 4 have been replaced with a set of contour plots, which have more quantitative information than the previously presented surface plot representations. Thus, for many reasons, the reader should ignore the results in Ref. 4 for the rack-in-pool geometry, and only utilize the data presented here in Figs. 9 – 12 as the correct total gamma flux distribution for this experimental configuration.

Specifically, Fig. 9 shows that, after about 10 cm from the rack face, the flux attenuates in the water as expected in nearly a pure exponential fashion and, as the tally volumes become further removed from the source, the fractional error begins to grow exponentially (again as expected). Close to the source, the y-directed dependence shows a peak just outside the source region and, in the xz plane, the spatial dependence of the flux is closely related to the spatial arrangement of the active Co-60 slugs within the rack configuration. In particular, Fig. 10 shows six regions of peak flux that correspond to the six active slugs in the axial direction, where a tapering off near the top and bottom slugs is also apparent. In the x-direction, there are two hot areas that are symmetrically placed around x = 0 that correspond to the two groupings of 8 pencils within the rack as shown in Figs. 7 and 8. The spatial resolution in the calculations is not sufficient to see the individual pencils, but the minimum associated with the separation caused by the two empty pencil locations in the center of the rack is clearly visible. Basically, all the observations here are exactly as expected.

Figures 11 and 12 show the same basic attenuation trends as Fig. 9, but this time, 2-D contour plots in the xy and zy planes are shown at the centerline of the rack in the transverse direction. These profiles again show the expected decrease in the flux with distance from the source. Figure 11 shows near perfect symmetry in the positive and negative x directions, since the model is indeed symmetric about the zy plane at x = 0. However, in Fig. 12, there is some slight asymmetry due to the aluminum plate that supports the rack on the -z side of the origin. Thus, the qualitative behavior observed here is easily explained, giving some measure of credibility to the base models. However, since no measured data are available for this geometry, no further benchmarking can be done at this time for this configuration.

The Gamma Cave Model and Associated Results

The gamma cave facility is a large-volume irradiation room that is located within a concrete cavity on one side of the reactor pool at the opposite end from the normal reactor position. A standard Co-60 rack, as described above, is placed within a sleeve/holder on the pool side of a ½ inch thick Al window. On the other side of the window is a large dry air-filled room where the samples to be irradiated, both large and small, are placed. Dose rates from 1 krad/hr to 1 Mrad/hr can be achieved by varying the distance from the Al window and the source strength of the C-188 sources placed within the rack holder. The initial 3 ft inside the window includes a 16″ high concrete shelf with tapered walls and ceiling so that the air volume expands from an area only slightly larger than the Co-60 rack area (roughly 24″×24″) to an area about 45″ high and 65″ wide. Beyond the shelf region is an irradiation volume with dimensions of 7′×8′×8.5′.

Several sketches from the actual MCNP model are shown in Figs. 13 – 15 that give a good view of the physical geometry for this system. In particular, Fig. 13 shows a side view (yz plane) of the gamma cave, with the shelf and tapered ceiling just inside the rack/window region readily apparent. Similarly, Fig. 14 gives a top view (xy plane) of the facility, clearly showing the tapered walls associated the shelf region and the large air volume that fills the rest of the room. Note that the air volume (pink color) in the back left portion of the room is the hallway leading to the gamma cave door. The door itself has not been model explicitly here -- it is simply treated as part of the exterior concrete wall (blue color) that completely surrounds the room. Several expanded views of the pool water, Co-60 rack, rack holder, and Al window regions are given in Fig. 15 to complete the overall MCNP gamma cave model. The geometry here is very similar to the rack-in-pool model described above, with the same Co-60 pencil description and gamma source distribution. In addition, the origin of the full gamma cave model is the center of the Co-60 rack (as it was for the rack-in-pool geometry).

This model was used to simulate the steady-state gamma flux distribution throughout the gamma cave facility and a series of flux distribution profiles, similar to those generated for the rack-in-pool geometry, are given below. However, we first note that silicon dose rates versus distance from the Al window are routinely measured within the gamma cave to fully characterize this system for the many users of the facility -- and these experimental data give an opportunity to partially validate the MCNP model generated in this work.

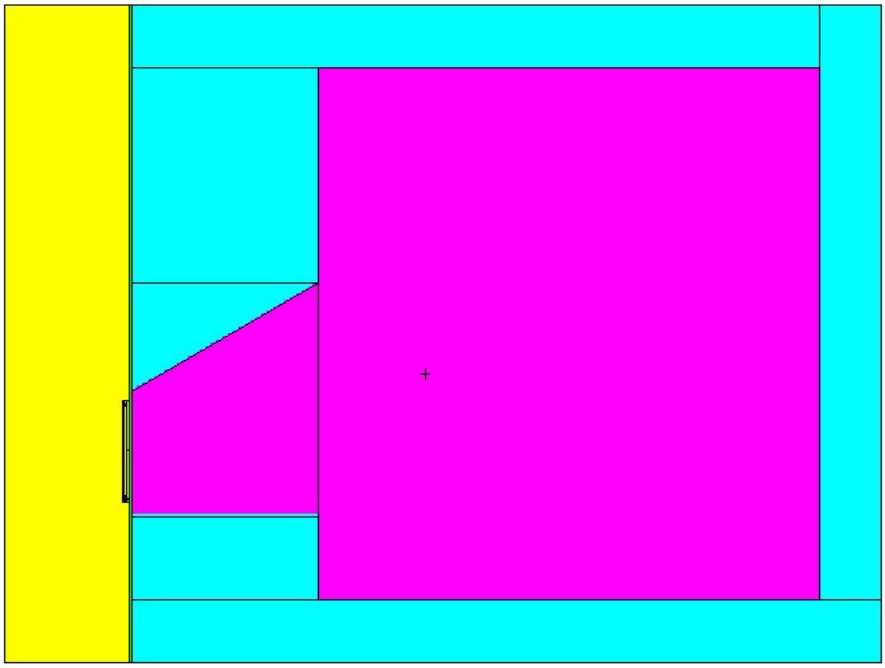

Fig. 13 Side view (yz plane) of the full MCNP gamma cave model (x = 0).

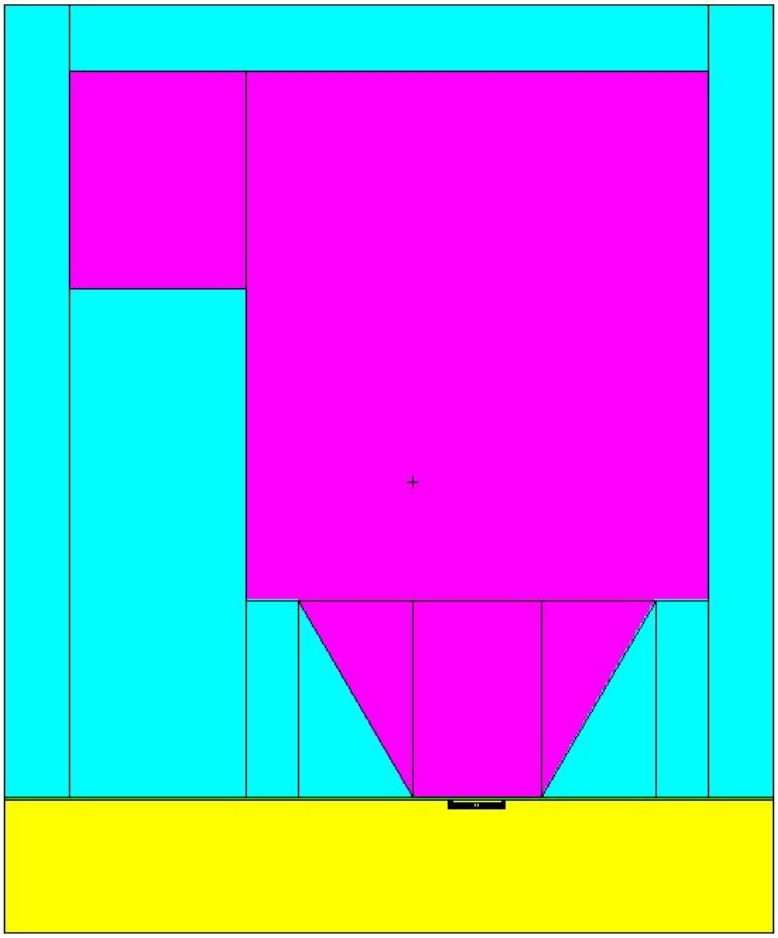

Fig. 14 Top view (xy plane) of the full MCNP gamma cave model (z = 0).

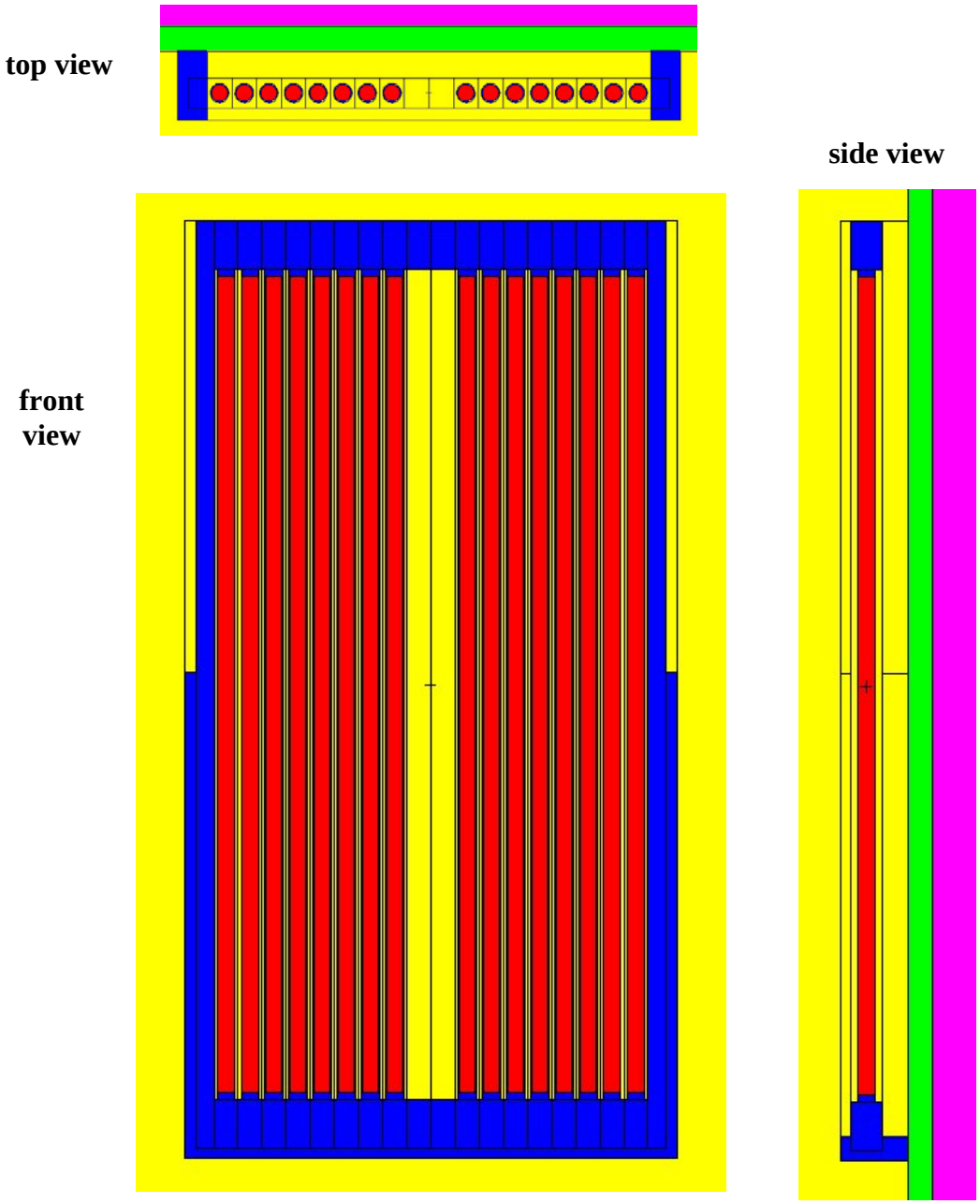

Fig. 15 Multiple expanded views of the Co-60 rack within the MCNP gamma cave model.

In particular, multigroup flux-to-dose conversion factors with 20 discrete groups from the BUGLE-96 shielding library (see Ref. 13) were used to convert the MCNP gamma fluxes into Si dose rates, and these were then compared to the measured dose rate data obtained in summer 2011. Using the half-life of Co-60, all the data (measured and computed) were adjusted to the end of October 2010 to correspond to the date of the experimental testing done within the gamma cave and reactor facilities. Only 12 groups of the available 20-group BUGLE-96 data were used, since the 1 – 1.5 MeV group (i.e. group 12) is the first one of interest in this study (both gammas emitted from Co-60 decay fall within this energy group).

Figure 16 shows a comparison of measured and calculated Si dose rates along the centerline of the facility, from just inside the Al window to very near the back wall (in both linear and logarithmic formats). Overall, the comparison is quite good, with excellent prediction of the attenuation profile (i.e. the shape of the curve) through nearly 10 ft of air (with the associated gamma scattering from the concrete walls). However, the magnitude of the MCNP results is consistently a little high relative to the measured values by roughly 30-35% or so. This discrepancy could be due to a number of factors such as the overall source normalization and distribution within the Co-60 rack, the measurement uncertainty (in both placement of the sample and the inherent measurement error), the use of dry air inside the gamma cave enclosure, the uncertainty in the concrete compositions, etc. -- where we note that only a small change in position and/or source normalization would make the measured and computed results become nearly identical. In all, however, Fig. 16 shows that the MCNP model does indeed give a good representation of the radiation field within the gamma cave, and that the results here should be sufficient for the analysis of other similar experiments within this facility.

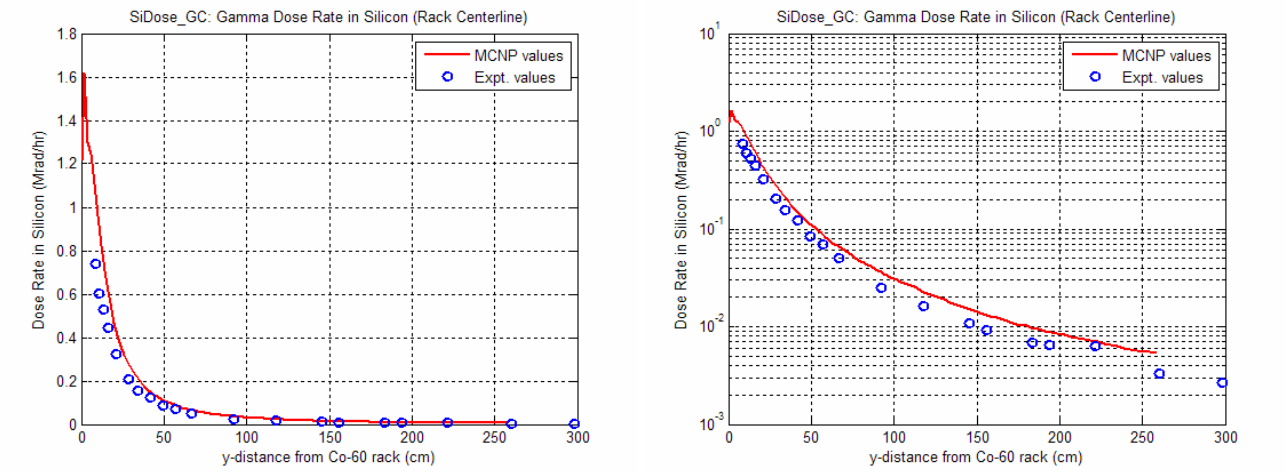

Fig. 16 Experimental and calculated Si dose rates vs. y along the centerline of the GC model.

With some validation of the base model, we now present results for the total gamma flux distribution in Figs. 17 – 20 (as was done previously for the rack-in-pool model). These data were generated using an ***fmesh*** tally in MCNP on a 2 cm mesh grid in each direction and processed/ plotted within Matlab (after 180 cm, the y mesh size was increased to 4 cm). Specifically, Fig. 17 gives the centerline flux values vs. distance from the source, and these clearly have the same basic shapes as the Si dose rate profiles shown above. The flux attenuates as expected in the air region, but the backscatter from the walls tends to reduce this somewhat. Also, although the fractional error

begins to grow as the tally volumes become further removed from the source, the overall statistical uncertainty here is very small (200×10^6 histories were simulated in the MCNP run).

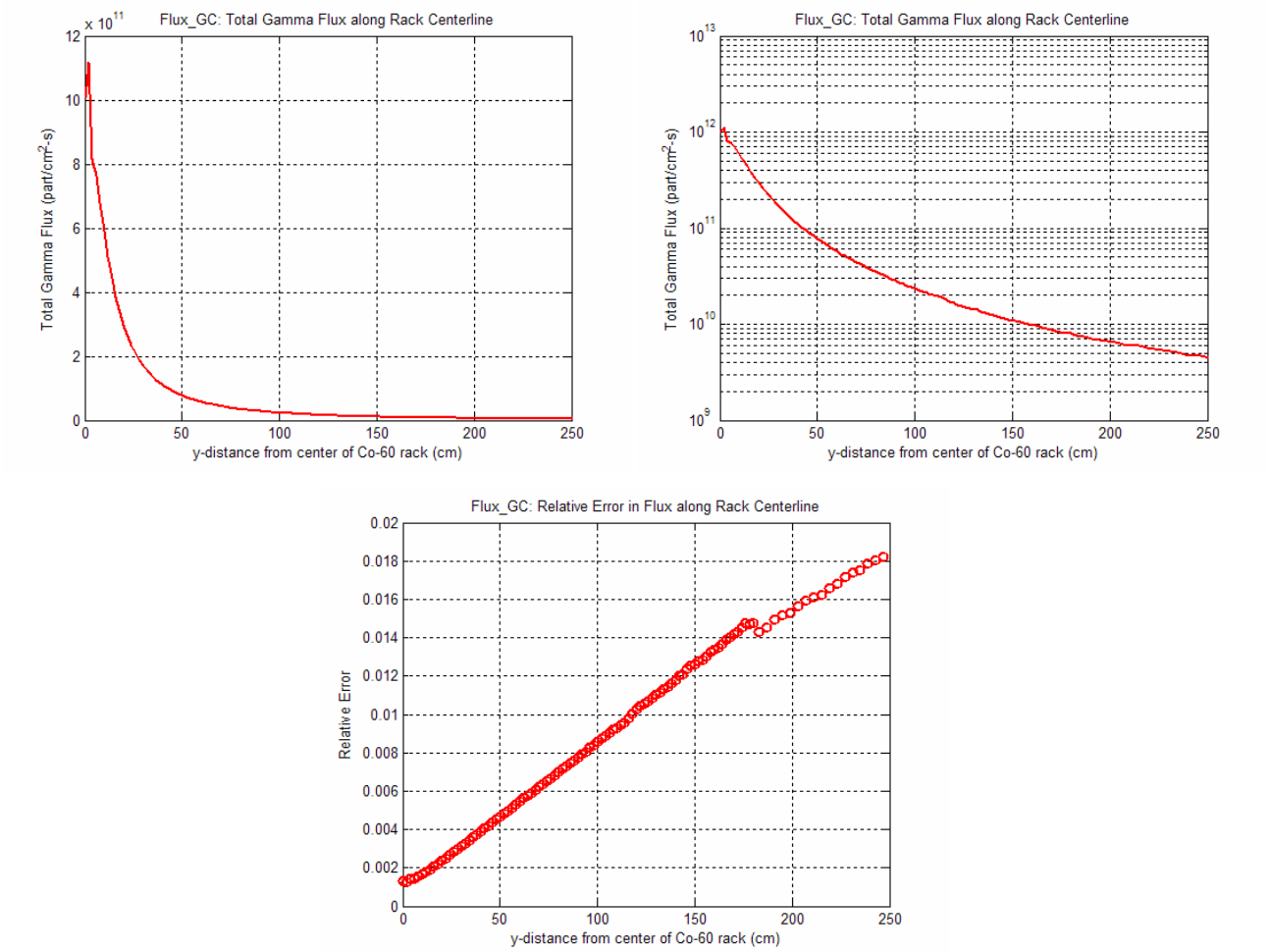

Fig. 17 Gamma flux and fractional error vs. y along the centerline of the GC model.

Close to the source, the y-directed dependence shows a peak just outside the source region and, as seen in Fig. 18, the spatial dependence of the flux in the xz plane is closely related to the spatial arrangement of the active Co-60 slugs within the rack configuration. This behavior is similar to that seen in Fig. 10 for the rack-in-pool model.

In Figs. 19 and 20, which show contour maps of the flux distributions in the xy and yz planes, we see the same basic attenuation trends as one moves radially and axially away from the source location. These profiles are basically as expected, where one can indeed see the effect of some of the structure associated with the concrete walls and ceiling of the gamma cave enclosure. For example, in the xy plane, Fig. 19 clearly shows the effect of the tapered side walls and, in the yz plane, Fig. 20 shows the impact of both the tapered ceiling and the concrete shelf (which extends to about 90 cm or so). Thus, the MCNP flux distributions obtained here do indeed behave as expected, and they give good qualitative and quantitative representations of the gamma field throughout the full facility.

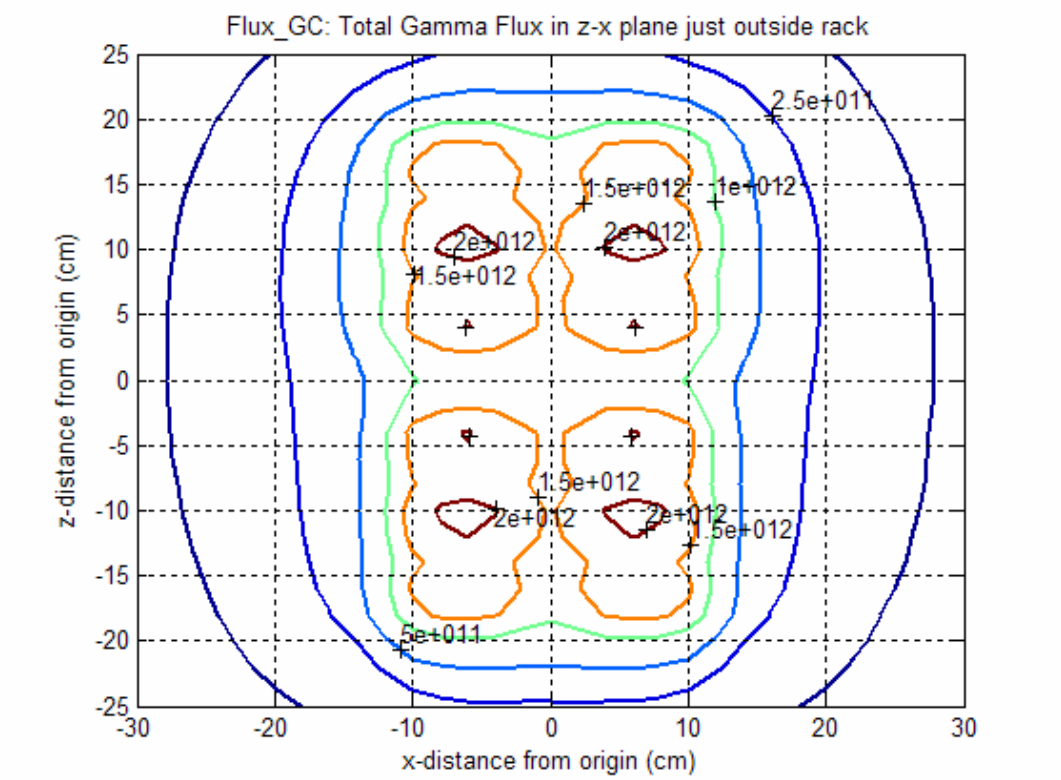

Fig. 18 Gamma flux distribution in the xz plane just outside the source region.

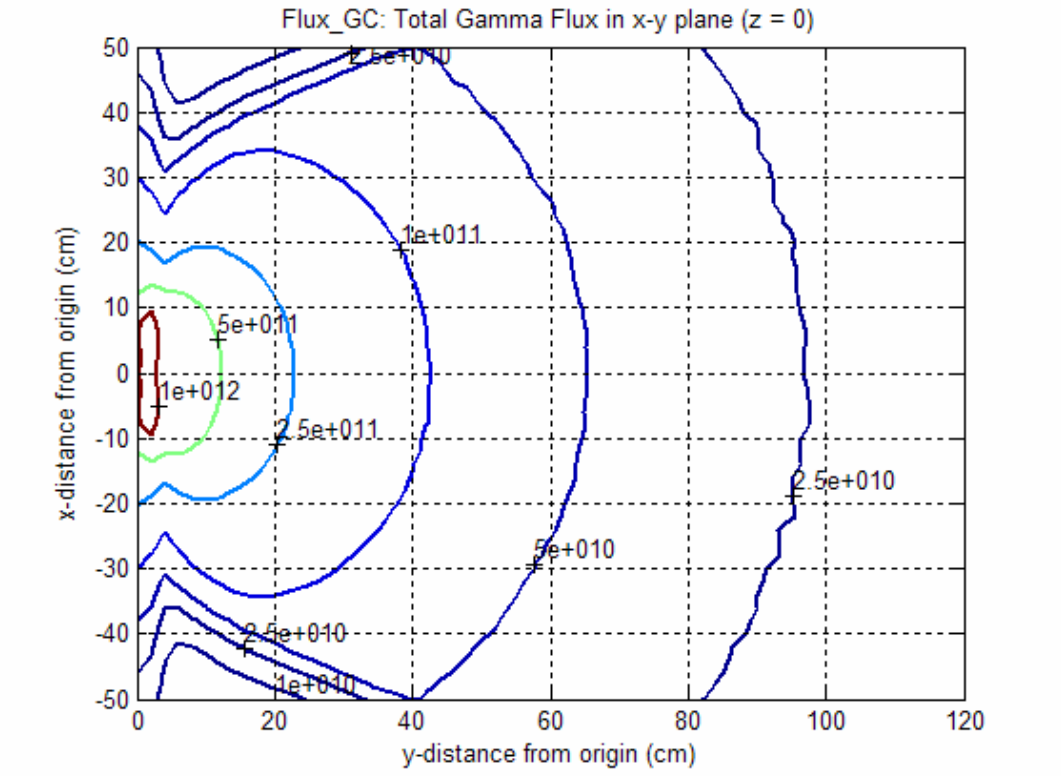

Fig. 19 Gamma flux distribution in the xy plane at z = 0 for the GC model.

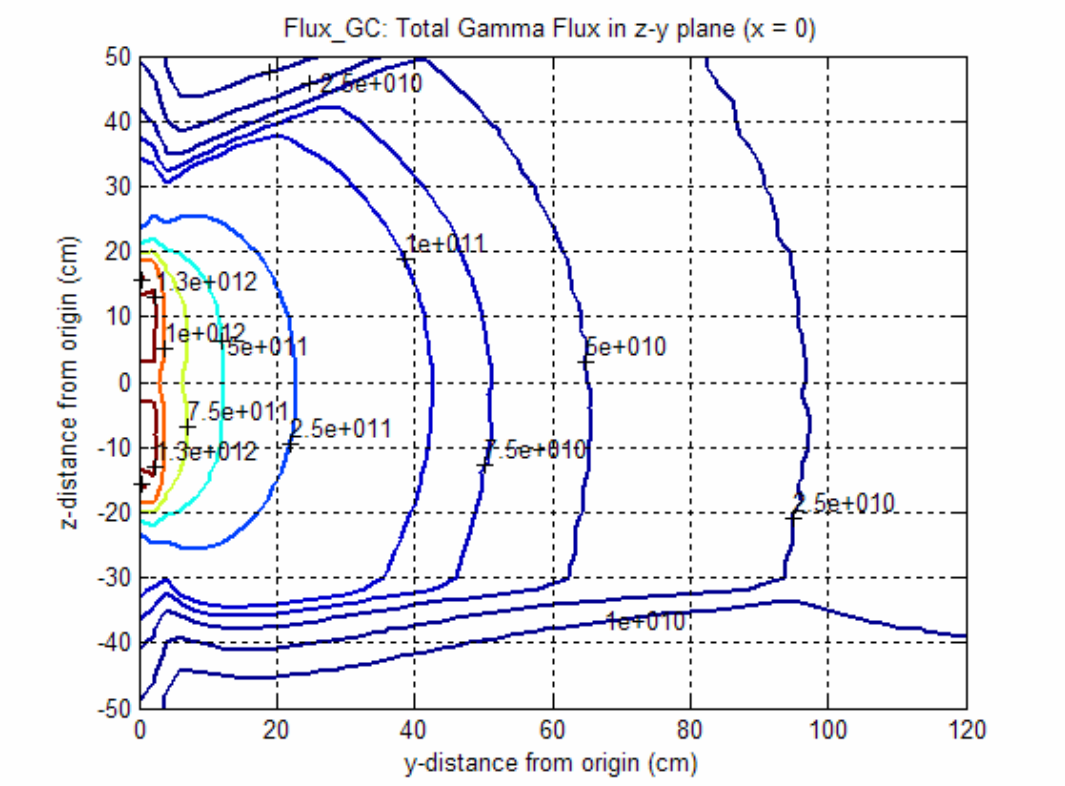

Fig. 20 Gamma flux distribution in the zy plane at x = 0 for the GC model.

Summary

Well, as noted in the introduction to this report, this document represents the Final Report for this project. The development of both the reactor models and the gamma irradiation facility models are complete, and the credibility of all the models have been established via comparison to measured data. Certainly some measurement vs. computation differences were observed but, in most cases, these are quite small, and they in no way detract from the functionality of the models to predict the radiation environments that are present within the reactor and Co-60 irradiation facilities. Overall, this project has been quite successful in its original goals, and the models developed here do indeed significantly enhance our local capability to analyze several of the key facilities within the UMass-Lowell Radiation Laboratory.

As a final deliverable for this project, in addition to the tabular and graphical results presented in this document, the main MCNP input decks for the reference cases and many of the input/output processing and mesh tally files from the various cases are also being distributed on CD (see the Appendix for a list of the files on the CD distributed with this report). Thus, the sponsor should have the capability to independently run the reference models and to modify these, as needed, to address their specific requirements. In general, there is a lot of untapped information available within the model results -- one just needs the time and motivation to extract some of this detail for a specific application of interest...

References

1. J. R. White, "Progress Report on MCNP Modeling for the UMLRR," informal in-house project documentation (Nov. 2010).
2. "J. R. White and R. Gocht, "Progress Report on MCNP Modeling for the UMLRR," informal in-house project documentation (Jan. 2011).
3. J. R. White, "Project Summary on MCNP Modeling for the UMLRR and Selected Gamma Irradiation Facilities," informal presentation given at the Naval Undersea Warfare Center, Newport, RI (March 2011).
4. J. R. White, R. Gocht, and M. Ducey, "Progress Report on MCNP Modeling for the UMLRR and for Selected Gamma Irradiation Facilities," informal in-house project documentation (August 2011).
5. J. R. White, et. al., "Calculational Support for the Startup of the LEU-Fueled UMass-Lowell Research Reactor," Advances in Reactor Physics and Mathematics and Computation, Pittsburgh, PA (May 2000).
6. J. R. White, et. al., "Preliminary Characterization of the Irradiation Facilities within the LEU-Fueled UMass-Lowell Research Reactor," Advances in Reactor Physics and Mathematics and Computation, Pittsburgh, PA (May 2000).
7. "Report on the HEU to LEU Conversion of the University of Massachusetts Lowell Research Reactor," submitted to the US Nuclear Regulatory Commission in fulfillment of Amendment No. 12 to License No. R-125 (April 2001).
8. J. R. White and L. Bobek, "Startup Test Results and Model Evaluation for the HEU to LEU Conversion of the UMass-Lowell Research," 24th International Meeting on Reduced Enrichment for Research and Test Reactors (RERTR 2002), San Carlos de Bariloche, Argentina (Nov. 2002).
9. J. R. White, et. al., "Design and Initial Testing of an Ex-Core Fast Neutron Irradiator for the UMass-Lowell Research Reactor," 2002 ANS Radiation Protection and Shielding Topical Conference, Santa Fe, NM (April 2002).
10. J. R. White, L. Bobek, and T. Regan, "Initial Testing of the New Ex-Core Fast Neutron Irradiator at the UMass-Lowell Research Reactor," UMass-Lowell Informal Project Documentation (June. 2002).
11. J. R. Lamarsh and A. J. Baratta, ***Introduction to Nuclear Engineering***, 3rd Edition, Prentice Hall (2001).
12. See http://www.nordion.com/documents/products/C-188_Brochure.pdf.
13. "BUGLE-96 - Coupled 47 Neutron, 20 Gamma-Ray Group Cross Section Library from ENDF/B-VI for LWR Shielding and Pressure Vessel Dosimetry Applications," Radiation Safety Information Computational Center, DLC-185 (1996).

Appendix

Listing of Selected Project Files
Distributed as part of Final Report Documentation

Documentation Files (both Word/PowerPoint and pdf formats):

preport_nov2010, preport_jan2011, project_summary_march2011, preport_july2011, finalreport_sept2011 -- this series of project report files may be useful for extracting various tables and figures, as needed.

Input, Mesh Tally, and Matlab and Excel Processing Files:

m13_BOL_MASTER.in, m25_BOL_MASTER.in, m25_BOL_deplready.in, m25_50MWd_MASTER.in -- these are the reference MCNP inputs for the four UMLRR cases (see Table 1 in the Final Report for k_{eff} values). These files have no experimental bayonets inserted within the geometry.

m13_fluxes.in, m13_BOL_fluxes.meshtal, m13_fluxes_mcnp.m -- files for generating the axial thermal flux profiles for the M-1-3 core (see Fig. 6 in the Final Report). Flooded bayonets are in locations C2, E2, and D5 and the required ***fmesh*** tallies are included.

umlblades.m -- Matlab file to generate a portion of the MCNP input file for the control blades in the various UMLRR models.

source_info.xls -- Excel file with information on the Co-60 source locations and magnitudes for the C-2 Co-60 rack.

co60_rack+water_2.in, co60_rack+water_2.meshtal -- final MCNP rack-in-pool model.

plot_jkmtal_p.m, flux_pool.m, sidose_pool.m, airdose_pool.m -- series of Matlab files to plot rack-in-pool mesh tally results (see Figs. 9 - 12 in Final Report)

rack+gc2.in, rack+gc2.meshtal -- final MCNP Co-60 rack + gamma cave model.

plot_jkmtal_gc.m, flux_gc.m, sidose_gc.m, airdose_gc.m -- series of Matlab files to plot gamma cave mesh tally results (see Figs. 16 - 20 in Final Report)